Twelfth Australasian Fluid Mechanics Conference
The University of Sydney, Australia 1995

SECONDARY JET INJECTION AT THE THROAT OF AN AXISYMMETRIC NOZZLE - DEDUCTION OF A VORTEX SKELETON

S.S. Vidakovic
Division of Building Construction and Engineering
C.S.I.R.O.
Highett, Victoria
Australia

R.E. Luxton
Department of Mechanical Engineering
The University of Adelaide
South Australia
Australia

ABSTRACT

An overexpanded axisymmetric convergent-divergent nozzle has been designed and manufactured to study the flow associated with a deflection of the jet caused by secondary flow injection normal to the primary flow at the throat. The secondary fluid injection produces an asymmetric jet downstream from the throat, which is deformed due to a Coanda like effect, to form a thin wall jet in the expanding part of the nozzle. When the jet approaches the nozzle exit, it does so as a relatively thin wall jet bounded by two counter-rotating streamwise vortices. These are associated with the deformation of the initially axisymmetric jet as it expands along the solid curved wall of the nozzle. When a small lip, in a form of an orifice, is placed at the nozzle exit it deflects the wall jet at a large angle across the nozzle axis. The flow studied is a continuation of the research initiated by Nathan and Luxton (1988) on the precessing jet from an axisymmetric Orifice-Cavity-Orifice nozzle configuration.

The flow exiting the convergent-divergent nozzle has been quantified using laser sheet flow visualisation, china clay surface flow visualisation, hot wire anemometry, pressure measurements and laser Doppler velocimetry. The china clay surface flow patterns reveal a footprint of two vortices on the diverging surface of the nozzle. The laser sheet flow visualisation has confirmed the presence of two counter-rotating streamwise vortices at the nozzle exit. A high rate of mixing in the region downstream from the throat inside the nozzle and at the nozzle exit is indicated by the level of the turbulent component in the velocity data. The turbulence intensities are greatest where the jet shear layer mixes with both the entrained ambient fluid and the fluid associated with the two streamwise vortices.

The flow topology was deduced from the surface flow patterns, laser sheet flow visualisation and static pressure data inside the cavity. As a consequence of the injection of the secondary fluid normally to the primary flow at the throat causes the primary jet to deform into an asymmetric wall jet.

The paper describes the deduction of the vortex skeleton inside the convergent-divergent nozzle and compares this with the vortex skeleton deduced to exist inside the nozzle when a cavity is added at the exit. Both qualitative and quantitative experimental data are used in the deduction process. The flow is complex, as is shown by the interpretation of the surface flow patterns and it is considered that this class of nozzle is worthy of further study.

INTRODUCTION

The ability to control thrust and vehicle orientation are very important factors in highly manoeuvrable rockets, missiles and tactical fighter aircraft. The agility of such a vehicle can determine the success or failure of its mission, especially for the air to air (AAM) or surface to air missile (SAM). Directional control of a conventional airborne vehicle is achieved by altering the position of the aerodynamic surfaces in the air stream to adjust the aerodynamic force vector. The alternative is to control the thrust by novel means. Presently vectoring of the thrust can be achieved in a number of ways: by inserting tabs, deflector plates or targets in the flow to deflect the thrust in a desired direction, or by modifying the physical shape of the nozzle. A novel way of vectoring thrust from a convergent-divergent nozzle is by fluid dynamic means. Injection of a secondary flow at the throat of a convergent-divergent nozzle, as investigated by Hussain and Clark (1981), causes the axisymmetric primary jet to be altered to exit the nozzle as a wall jet. In the present study it is shown that when a small lip is introduced at the exit of the nozzle, the wall jet is deflected at a large angle across and away from the axis as it leaves the nozzle, in a manner similar to that discussed by Nathan and Luxton (1992). A fully instrumented nozzle was manufactured to study flow in the convergent-divergent geometry and the effects of a specific length cavity attached to the nozzle exit on the thrust, angle of deflected jet and general flow structure has been determined. A number of pressure ports were located axially and circumferentially to allow evaluation of static pressure in the nozzle and cavity. The cavity was made from acrylic permitting flow

visualisation and laser Doppler velocimetry (LDV) to be implemented. A number of surface flow visualisation techniques, Roshko (1991) and Nakayama, Woods and Clark (1988), were also employed to determine the flow structure inside the nozzle. With the results from the velocity measurements, pressure distribution and flow visualisation, a vortex skeleton has been deduced for a nozzle with and without a cavity.

APPARATUS

The experiments in this study were performed on an overexpanded convergent-divergent nozzle, shown in Figure 1, with and without a 100 mm long transparent cavity, attached to the nozzle exit. CD nozzle here is defined as a convergent-divergent nozzle with a smooth contraction from 25 mm diameter air supply line to a 10 mm diameter throat, followed by a smooth expansion to 60 mm diameter. The nozzle profile follows a curve ;

$$y = C_1 \sin (C_2 x)^{1.5} + C_3$$

where C_1, C_2 and C_3 are constants. The CD10 nozzle here is defined as a convergent-divergent nozzle with a 100 mm cavity attached at the nozzle exit. The joint between the nozzle and cavity is a smooth transition. A fluid dynamic disturbance in the nozzle was produced by introducing secondary flow through one of four equally spaced 2 mm diameter ports at the throat such that the secondary jet is normal to the primary flow. This jet causes and maintains asymmetric flow downstream from the throat. The primary mass flow rate was regulated by a valve and measured using an orifice plate flow meter. The LDV measurements were taken using a 2 velocity component 5 Watt Argon-ion laser. A sharp edged orifice, attached to the nozzle exit, deflected the jet across and away from the nozzle axis. Eight exit orifice plates were examined, ranging from 55 to 20 mm diameter, in 5 mm increments.

PROCEDURE

Several types of flow visualisation technique were used here: china clay and oil flow visualisation on the surface and laser sheet particle illumination in the flow itself. The china clay surface flow visualisation method is usually implemented by applying a thin film of a solution of "china clay", (Kaolin in a light oil), to the inner nozzle surface. As the solution dries it leaves an opaque white surface. When oil of wintergreen is applied to this surface, by spraying, it matches the refractive index of china clay, thereby making it appear transparent. The flow is then started and the surface flow patterns can be visualised by following the motion of the slurry as it dries. The regions of high mass transfer have a high rate of evaporation and those areas return to the opaque white state first. The areas of separation have the slowest evaporation and therefore dry more slowly. By taking still photos of the various stages of the process, critical points can be determined, Perry and Chong (1987), Perry and Fairlie (1974), and the topology determined, Tobak and Peake (1982). A variation of the method yields dark areas in regions of high shear and opaque areas where shear is small, Nathan (1988). The oil streak surface flow visualisation is implemented either by applying a film of oil to the surface and starting the flow, or by introducing the oil at the nozzle throat through one of the secondary flow injection points, Vidakovic (1995) and Su (1989). The oil that is moved by the shear stress, accumulates in the areas of separated flow or other low shear or low mass transfer regions. The flow direction on the surface can be determined by the oil droplet orientation. The advantage of this method over china clay is that the amount of oil introduced at the throat can be varied to follow the flow pattern development, and images can be captured using a conventional 35 mm camera.

Laser sheet particle illumination was implemented by seeding the flow well upstream from the throat using a "six-jet atomiser", Vidakovic (1995), which produced well mixed very fine water droplets. The water vapour laden air jet was illuminated using a laser sheet and images were captured on film using a conventional 35 mm camera. The laser sheet was introduced either parallel to or normal to the nozzle axis to observe structures in both planes.

The velocity measurements were acquired using LDV and hot wire anemometry. LDV measurements were performed by traversing the intersection of the laser beams at whose intersection point measurements taken, across the flow. The procedure was time consuming since over 4000 points was required, at that point in space, to obtain a time averaged 2 component velocity vector and associated turbulence intensity. A constant temperature hot wire velocity measurements were obtained using a 5 μm diameter, 2.0 mm long Tungsten wire element.

Both static and dynamic pressure measurements were taken inside and outside the nozzle. Static pressure ports, 4 of which were located at the throat, 16 azimuthally distributed 60 mm upstream from the nozzle exit and 7 axially aligned equally distributed as shown in Figure 1., allowed detailed surface pressure profiles to be obtained from an array of differential pressure transducers with a resolution of 0.1% of full scale deflection of ± 4 kPa.

RESULTS

In the case of the CD nozzle, it was found that for a Reynolds number below 35,000, the flow separates axisymmetrically downstream from the throat, in the absence of any asymmetrical disturbance. Between 35,000 and 45,000, the primary jet can separate either axisymmetrically or asymmetrically downstream from the throat. The flow separated asymmetrically for Reynolds numbers above 45,000 with its azimuthal direction changing randomly. The azimuthal direction can be fixed by injecting secondary fluid at the throat, as long as the secondary mass flux is above a minimum which has been found necessary to maintain the stable flow condition. The asymmetric flow can be produced at much lower Reynolds numbers by injecting secondary fluid. The asymmetric flow produces a pair of streamwise vortices, clearly visualised by a laser sheet normal to the nozzle axis illuminating water vapour laden fluid as shown in Figure 2. The two stream surface bifurcations extending from the throat to the two foci are visible in both Figure 3 and 4. This flow pattern appears to be produced by the expansion of the primary flow laterally around the transverse curvature of the nozzle and interaction with the ambient fluid which is induced into the nozzle.

When an exit ring was placed at the nozzle exit, the primary wall jet was deflected across the nozzle axis due to an impingement of the wall jet on the exit lip. This reduced the available exit area for the ambient fluid to be induced and therefore increased its velocity as it is induced into the nozzle. Streamlines are tightly curved as the induced fluid

negotiates the exit lip. These features evidence a strong radial pressure gradient and this acts to deflect the primary jet further. A portion of the primary fluid was recirculated back into the nozzle by the exit ring and this fluid feeds into the vortex, as shown by surface flow visualisation in Figure 3(a). An interpretation of the flow is shown in Figure 3 (b). With a decrease in the exit area, the amount of primary fluid recirculated back toward the throat increases. As a consequence the foci and the negative stream surface bifurcation, which feeds into the vortex, moves away from the exit lip supporting the postulate that more of the primary fluid is recirculated. The evidence indicates that the vortex strength increases with the reduction of exit area, at least within the range of area ratios tested. It has been confirmed independently, by measuring static pressure inside the nozzle, that for a reduction of exit area the amount of ambient fluid induced is zero as the area ratio (AR) approaches the value of 0.34 which coincides with the maximum angle that the jet is deflected at, being 80 degrees, for the CD nozzle. This however coincides with a lower exit velocity and a lower thrust discussed elsewhere, Vidakovic (1995) and this supports the postulate that more of the primary fluid is recirculated. This is followed by an increase in static pressure as the AR is reduced below 0.34. Figure 4 shows a captured image of the surface flow patterns in the CD nozzle showing an induced ambient fluid surface flow pattern, as viewed along the nozzle axis toward the throat, occupying about 60% of the area for a Re = 72,000 and AR = 0.83 . The surface flow patterns for the same Re but AR = 0.34, shows the reduced area of the induced ambient fluid surface flow patterns, now occupying only about 40% of the area viewed. Details of these findings may be found in Vidakovic (1995). Interpretation of the flow pattern inside the CD nozzle topologically to the derived vortex skeleton as shown in Figure 5. The general flow picture in the CD nozzle consists of the two negative bifurcation surfaces produced by the interaction between and mixing of the primary and entrained ambient fluids, two further negative bifurcation surfaces which arise from interaction between and mixing of the primary fluid and the recirculated portion of primary fluid and two foci into which the negative bifurcations feed. It is postulated that these foci are the footprints of a strong vortex loop which passes over the primary fluid wall jet providing the interface with the induced ambient fluid which flows into the nozzle. This postulate applies for CD and CD10 nozzles. The surface flow patterns are similar to the surface flow patterns produced in the CD10 nozzle Vidakovic and Luxton (1991) for which it was possible both to view and measure through the cylindrical cavity extension. As the exit area was reduced in the CD10 nozzle, the foci appeared to move upstream toward the throat and were pushed apart by the spreading wall jet. This was attributed to the large recirculation of the primary fluid imposed by the exit lip. It is now postulated that it is the recirculation of the high momentum fluid which produces the increase in vortex strength, as indicated in the interpretation shown in Figure 6.

CONCLUSION

The flow mechanism inside the CD nozzle has been identified from a combination of flow visualisation, pressure and velocity measurements. This has been compared with that of the CD10 nozzle. The vortex skeleton has been deduced from quantitative and qualitative data derived from china-clay surface flow visualisation and laser sheet particle illumination. The characteristic flow inside the nozzle has been validated independently by the use of pressure and velocity data. The deflected jet angle has been characterised in terms of lip height and the effect of lip height on vortex strength has been noted.

The efficient deflection of the wall jet at the exit from the CD and CD10 nozzles is due to a combination of lip height and the radial pressure gradient produced by a strong vortex line inside the nozzle, just upstream from the exit lip. This vortex line stretches across the exit diameter and joins the two foci described. The addition of a larger lip produces a stronger vortex and hence a stronger radial pressure gradient resulting in a larger deflection of the exiting jet. The maximum deflection is reached when a balance between the radial pressure gradient and the exiting flow momentum is reached.

REFERENCES

[1] **Bradshaw, P.** (1983) "Complex three-dimensional turbulent flows", 8th A.F.M.C., pp k5.1-k5.7.

[2] **Hussain, A.K.M.F. and Clark, A.R.** (1981) "On the coherent structure of the axisymmetric mixing layer: a flow-visualisation study", J.F.M., vol 104, pp 263-294.

[3] **Nakayama, Y., Woods, W.A. and Clark, D.G.** (1988) "Visualised Flow: Fluid motion in basic and engineering situations revealed by flow visualisation", Pergamon Press, 1988.

[4] **Nathan, G.J.** (1988) "The Enhanced Mixing Burner", Thesis for the Degree of Doctor of Philosophy, The University of Adelaide, Mechanical Engineering Department.

[5] **Nathan, G.J. and Luxton, R.E.** (1992) "The flow field within an axi-symmetric nozzle utilising a large abrupt expansion", Recent Advances in Experimental Fluid Mechanics, ed. F.G.Zhuang, International Academic Publication, pp 527-532.

[6] **Perry, A.E. and Fairlie, B.D.** (1974) "Critical points in flow patterns", Adv. in Geophysics B 18:, pp 219-315.

[7] **Perry.A.E. and Chong, M.S.** (1987) "A description of eddying motions and flow patterns using critical-point concepts", Ann.Rev.Fluid Mech., vol 19, pp 125-155.

[8] **Roshko, A.** (1991) "Uses of flow visualisation in research", I.C.E.F.M., pp 3-11.

[9] **Su.Y.** (1989) "Mechanism of sidewall effect studied with oil flow visualisation", A.I.A.A. Journal, vol 27, No.12, pp 1828-1830.

[10] **Tobak, M. and Peake, D.J.** (1982) "Topology of three-dimensional separated flows", Ann.Rev.Fluid Mech.14, pp 61-85.

[11] **Vidakovic, S.S. and Luxton, R.E.** (1991) "Fluid mechanics of deflected jets: Flow visualisation within the nozzle", I.S.T.P.4 in Heat and Mass Transfer, pp 50-62, July 14-19 1991, UNSW, Sydney, Australia.

[12] **Vidakovic, S.S.** (1995) "Fluid dynamic means of varying the thrust vector from an axisymmetric nozzle", Thesis for the Degree of Doctor of Philosophy, The University of Adelaide, Department of Mechanical Engineering.

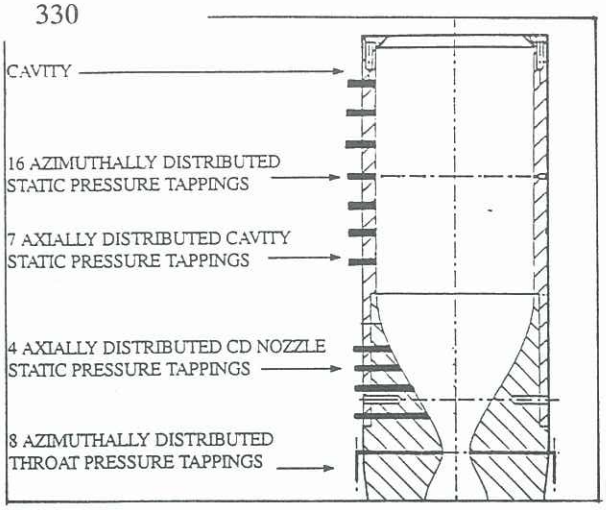

Figure 1. Schematic of the convergent-divergent nozzle and pressure tapping locations.

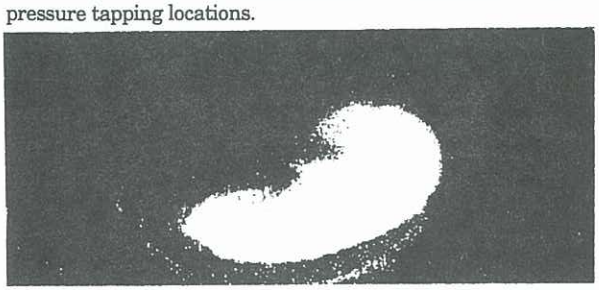

Figure 2. Wall jet cross-section visualised by laser sheet 10 mm above the exit plane, CD nozzle without the exit ring, showing streamwise vortices.

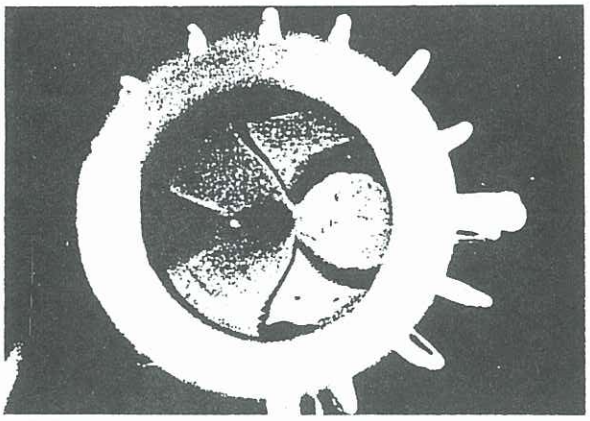

Figure 3 (a) oil-surface flow patterns inside CD10 nozzle near the throat, jet exiting from left to right at Re = 72,000 and AR = 0.69

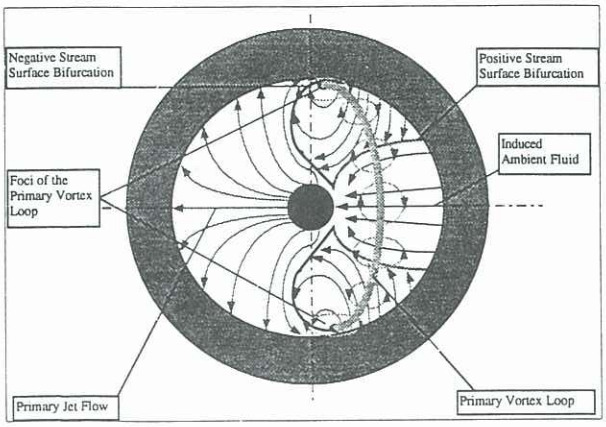

Figure 3 (b) Interpretation of the oil-surface flow patterns at Re = 72,000 and AR = 0.69

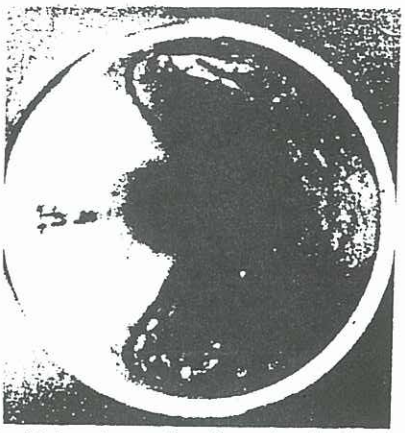

Figure 4. China clay surface flow visualisation inside CD nozzle at Re = 72,000 and AR = 0.69

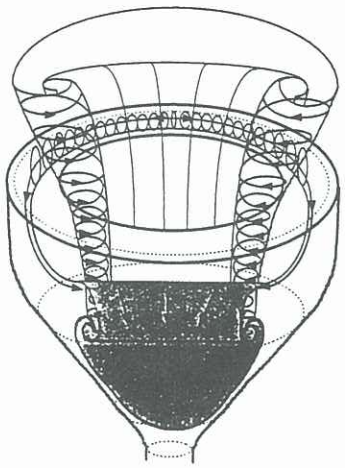

Figure 5. Schematic of the postulated vortex skeleton inside the CD nozzle with moderate lip at the exit causing the wall jet to deflect.

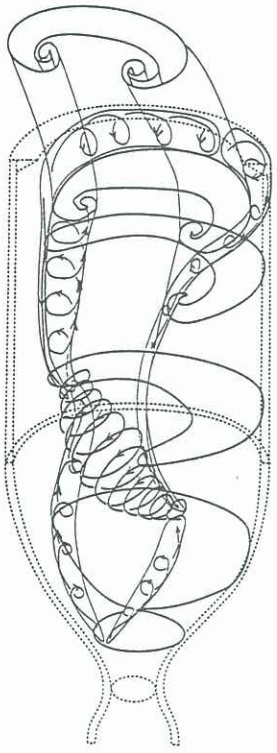

Figure 6. Schematic of a deduced vortex skeleton built from the interpretation of the surface flow visualisation figures inside the CD10 nozzle, showing vortex loops.